08,16

Electrical properties of tandem solar cells based on films of organic-inorganic perovskites deposited on thin-film silicon solar cells

© G.V. Nenashev[1], N.A. Fokina[1,2], M.S. Dunaevskiy[1], A.N. Aleshin[1]

[1] Ioffe Institute,
St. Petersburg, Russia
[2] St. Petersburg State Electrotechnical University „LETI",
St. Petersburg, Russia

E-mail: virison95@gmail.com

Received December 14, 2023
Revised December 14, 2023
Accepted December 25, 2023

This study presents an analysis of the morphological and electrical properties of multilayer structures fabricated using thin films of organometallic halide perovskites (OHP), specifically $CH_3NH_3PbI_3$, deposited onto the surface of crystalline silicon (*c*-Si)-based solar cells. The structural morphology and electrical characteristics of these multilayered configurations were investigated through atomic force microscopy (AFM), current-voltage (I-V) characterization, and impedance spectroscopy. The AFM observations revealed significant morphological variations among the produced samples. I-V analysis conducted at 300 K indicated that all samples exhibited enhanced photoconductivity relative to pure *c*-Si, suggesting a beneficial influence of the perovskite layer. Impedance spectroscopy analysis revealed that in the absence of light, a sample with a perovskite layer on *c*-Si displayed two semicircles in its Nyquist plot, implying the coexistence of two distinct processes, such as ion diffusion or charge recombination. These processes appear to converge into a single mechanism upon exposure to light, a change attributed to the altered concentration of charge carriers. The findings of this research pave the way for further optimization and enhancement of the performance parameters of advanced tandem *c*-Si solar cells with top layers composed of organometallic halide perovskites.

Keywords: impedance spectroscopy, electrical conductivity, solar cells, organic-inorganic perovskites, crystalline silicon.

DOI: 10.61011/PSS.2024.02.57922.271

1. Introduction

Modification of the surface of *c*-Si solar cells (SCs) with films of organic-inorganic absorption coefficient in these materials in the visible region of the spectrum [2], the possibility of forming multilayer heterostructures [3], sufficiently high mobility of charge carriers [4], as well as relatively low production costs. Currently, the maximum efficiency of solar cells based on silicon heterostructures (HIT) reaches 26.8% [5]. The most promising combination of manufacturing technology and energy conversion efficiency are tandem SCs. A conventional perovskite SC is a structure in which a thin layer of organic-inorganic perovskite is used as an active layer to absorb light and convert it into photocurrent. A tandem SC consists of two or more layers of photovoltaic material deposited in series (sandwich structure), one of which is a perovskite. The main difference between a conventional perovskite SC (PSC) and a tandem SC is their efficiency. The efficiency of tandem SC is significantly higher than that of conventional SC, which is due to that the tandem structure absorbs over a wider range of the solar spectrum, resulting in a larger portion of solar energy being converted into electricity.

The efficiency of tandem SCs, based on *c*-Si and organometallic perovskites, is rapidly increasing. In 2018 the unprecedented efficiency of such structures was 25.2%, and in 2020 it was raised to 27.7%, and then to 29.15%. In 2021 this index approached 30% and amounted to 29.8%. In 2022 researchers from the Ecole Polytechnique Federale de Lausanne (EPFL) and the Swiss Center for Electronics and Microtechnology (CSEM) developed tandem SCs with efficiencies of 30.93% and 31.2%, respectively [6] (33.2% in 2023). These results confirm that the development and study of perovskite SCs deposited on the surface of *c*-Si SCs is an actual and promising direction.

One of the effective methods for studying tandem SCs is the impedance spectroscopy (IS) method. IS is a universal characterization method for monitoring ongoing electrical and electrochemical processes, as well as profiling the electronic structure in solid-state devices [7]. IS is considered as a fast, non-invasive and inexpensive method that allows you to study SC parameters to research and improve its performance. Although the impedance parameters of perovskite tandem SCs exhibit a wide variety of characteristics [8], interpreting such spectra is a challenging task. One of the reasons for the problem of interpreting IS data is the difficulty of taking into account the influence of ion movement in the perovskite layer. Mobile ions can cause surface polarization of the interface [9], affecting charge

transfer rates or causing capacitive accumulation of charge carriers.

Another important characteristic of perovskite films is their surface morphology. Improving the morphology and crystallinity of organic-inorganic perovskite layers is a key factor for reducing defect density, leakage currents and contact resistance, which leads to the creation of more stable and efficient SCs [10]. The main goal of morphology monitoring is to obtain films with lower roughness, better uniformity, compactness and the absence of point defects.

This paper presents the results of a study of the morphological and electrical properties of multilayer structures created on the basis of thin films of organometallic halide perovskites (OHP), $CH_3NH_3PbI_3$ deposited on the surface of SC based on crystalline silicon (*c*-Si). The morphology and electrical properties of these structures were studied by AFM, current-voltage characteristics, and impedance spectroscopy. It was shown that the studied samples demonstrate noticeable photoconductivity, and the photoconductivity of samples with a top perovskite layer OHP1/*c*-Si and OHP2/*c*-Si significantly exceeds similar characteristics for SCs based on *c*-Si.

2. Objects and methods of study

During the synthesis of organometallic halide perovskites, two solutions were prepared. The first solution was prepared by mixing methyl ammonium iodide (CH_3NH_3I) and dimethylformamide (DMF) in the ratio 1 : 3. A similar ratio 1 : 3 was used to prepare a second solution in which lead iodide (PbI_2) and DMF were mixed. Next, 4.62 g of PbI_2 were mixed with 1.58 g of CH_3NH_3I. The resulting mixture was stirred using a magnetic stirrer for 12 h at a temperature of 80°C. At the next stage of the synthesis of organometallic halide perovskites the solution was purged with argon at a temperature of 100°C for more than eight hours in order to remove the solvent. As a result, a concentrated, viscous, dark brown solution of organometallic perovskite was obtained. The resulting solution was designated as sample OHP2 and deposited on a silicon substrate (OHP2/*c*-Si).

A solution of barium iodide in DMF was prepared using commercial barium iodide dihydrate powder. In the initial stage involved drying this powder at a temperature of 100°C for 24 h to obtain anhydrous barium iodide. Then the dehydrated crystalline substance was completely dissolved in DMF until the solution concentration reached 5%. This barium iodide solution was then mixed with an existing organometallic perovskite solution consisting of $CH_3NH_3PbI_3$. The concentration of barium ions in the perovskite solution could vary from 1% to 3%, depending on the initial components. This solution, designated as $CH_3NH_3Pb_{0.98x}Ba_{0.02x}I_3$ was deposited on silicon substrate and designated as OHP1/*c*-Si.

To measure the electrical characteristics, SCs made of single crystal silicon *c*-Si, provided by the Center for Thin Film Technologies in Energy, were used. The main SC includes a crystalline substrate of n-type silicon, *c*-Si, oriented (100). Layers of amorphous hydrogenated silicon carbide in the form of a solid solution $Si_xC_{x-1}:H$ with $0.8 < x < 0.9$ 0.5–2 nm thick, as well as an undoped layer of amorphous hydrogenated silicon 2–5 nm thick were sequentially deposited on both sides of the substrate. A doped *p*-layer of amorphous hydrogenated silicon 5–20 nm thick and layer of indium tin oxide (ITO) 90–110 nm thick [11–13] were deposited on the front side (radiation side), a doped *n*-layer of amorphous hydrogenated silicon 10–20 nm thick and ITO layer 40–80 nm thick were alternatively deposited on the back side of the crystalline substrate. The crystalline substrate 80–250 μm thick is the component in which the main light absorption in SC occurs. Perovskite solutions were deposited onto *c*-Si substrates by spinning using KW-4A Chemat centrifuge at a speed of 2000 rpm for 30 s. Basis SC with a top layer of organometallic perovskite $CH_3NH_3PbI_3$ is shown in Figure 1.

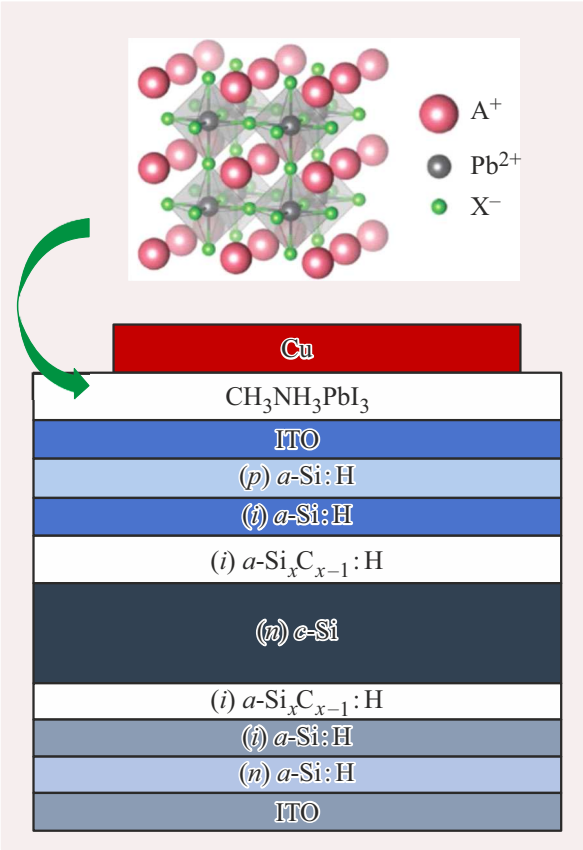

Figure 1. Basis SC with a top layer of organometallic perovskite $CH_3NH_3PbI_3$.

Structure and thickness of films $CH_3NH_3PbI_3$ were studied by atomic force microscopy (AFM) using NTegra-Aura (NTMDT-SI, Russia) microscope and NSG10 probes (TipsNano, Russia). To study the solutions $CH_3NH_3PbI_3$ were deposited on polished silicon substrates with a resistivity of 20–40 $\Omega \cdot$ cm.

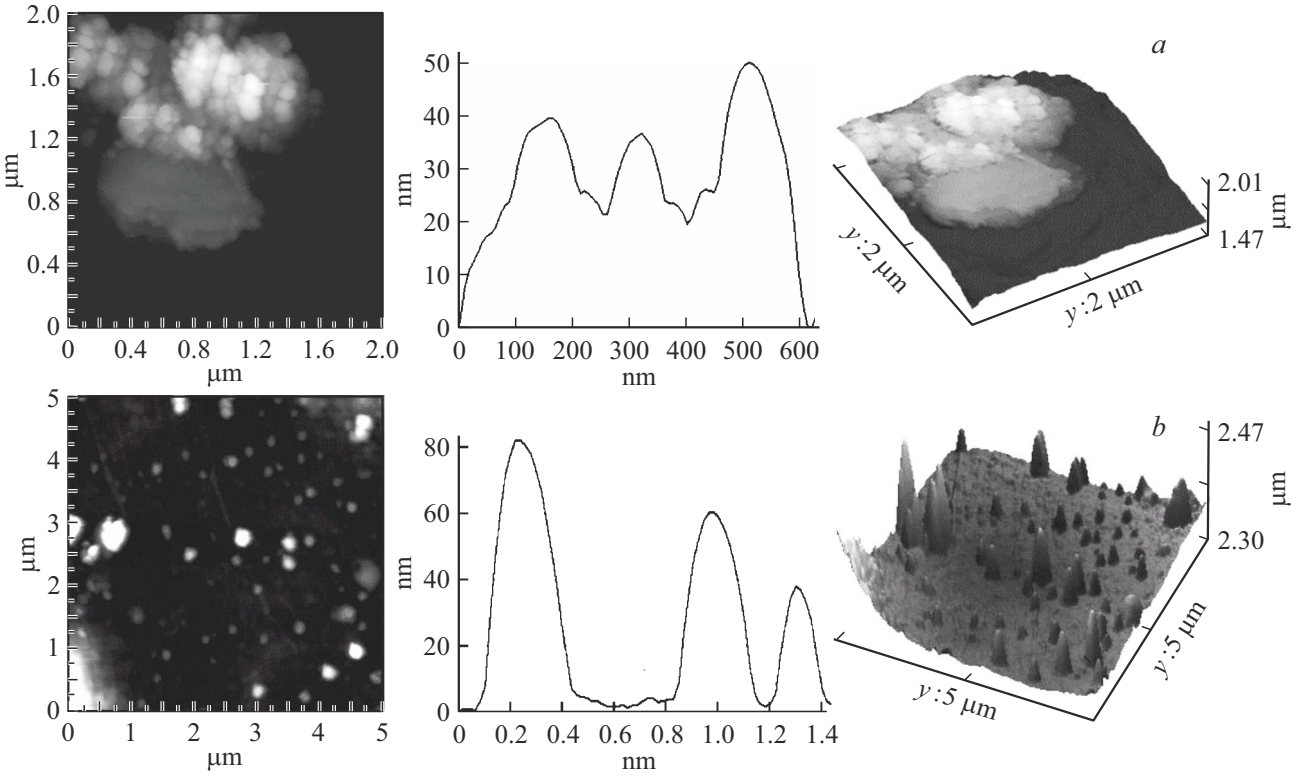

Figure 2. AFM images of topography (left row), section profiles (central row) and 3D relief surface (right row) of samples OHP1/*c*-Si (*a*) and OHP2/*c*-Si (*b*).

Current-voltage characteristics (I-Vs) of samples were measured in planar geometry using a two-probe scheme. The experiments were carried out in the dark and under illumination with solar radiation simulator using an automated measuring system based on Keithley 6487 picoammeter and adjustable voltage source AKIP-1124, the voltage varied in the range of -2 to $+2$ V [14].

A set of measurements using impedance spectroscopy was carried out in the dark and under illumination with sunlight simulator using Elins Z-500PX, impedance meter in accordance with the technique described in our previous paper [15]. The top electrode was made of copper. The experiments were carried out at a forward bias from 0 to 1 V and in the frequency range from 10 Hz to 0.5 MHz. To minimize external interference, samples were placed in a copper insulated box.

3. Results and discussion

To study the surface morphology of the samples OHP1/*c*-Si the AFM method was used, the results of which are presented in Figure 2. It was found that the surface of the samples has a complex and rough structure with the presence of globules with well-defined boundaries, which indicates the heterogeneity of the perovskite layer. Besides, irregularities were identified about 100 nm wide and height in the range 20–30 nm (RMS roughness is 30 nm). Surface analysis of sample OHP2/*c*-Si using AFM showed the presence of partially smooth areas with irregularities ranging in size from 200 to 300 nm in width and from 40 to 80 nm in height (RMS roughness is 15 nm).

Compared to sample OHP2/*c*-Si, the sample OHP1/*c*-Si is characterized by a more complex and uneven morphology. Such irregularities and heterogeneity can affect electron transport by creating obstacles that potentially reduce electrical conductivity. Sample OHP2/*c*-Si, on the contrary, has a relatively smooth surface with less roughness, which can have a beneficial effect on conductivity. A smoother surface can facilitate the electron scattering reducing and, as a result, provide more efficient transport of charge carriers. This, in turn, can lead to increase in the electrical conductivity of the sample OHP2/*c*-Si compared to the sample OHP1/*c*-Si.

I-Vs of samples OHP1/*c*-Si, OHP2/*c*-Si and *c*-Si, obtained at forward and reverse bias, in the dark and under illumination with sunlight simulator, are presented in Figure 3, *a*–*c*. As follows from Figure 3, *a*–*c*, I-Vs linearity is observed only for sample OHP1/*c*-Si in the absence of illumination; in other cases, I-Vs demonstrate nonlinearity with both signs of bias. All three samples demonstrate noticeable photoconductivity, and for the samples OHP1/*c*-Si and OHP2/*c*-Si it significantly exceeds the similar characteristics for the *c*-Si sample. This may indicate that the perovskite layer significantly improves the photoconductivity of the original substrate. Differences in electrical conductivity were also discovered: the conductivity of the samples OHP1/*c*-Si

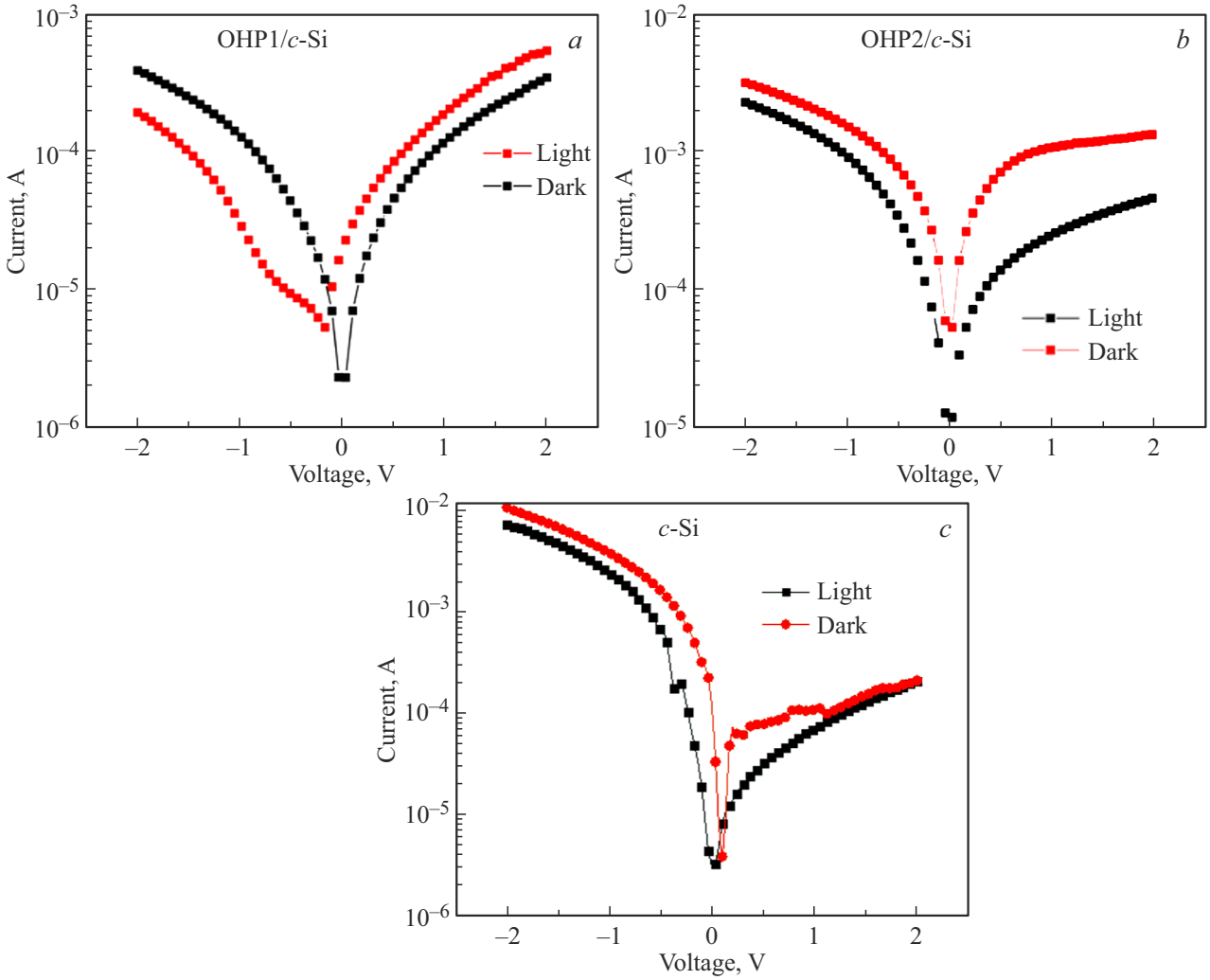

Figure 3. I-Vs of samples OHP1/*c*-Si (*a*), OHP2/*c*-Si (*b*) and *c*-Si (*c*) obtained in dark and upon illumination by sun light simulator.

and OHP2/*c*-Si under a forward bias increases significantly, while under reverse bias it decreases compared to the sample *c*-Si. At the same time, the conductivity of the sample OHP2/*c*-Si at both types of bias significantly exceeds that of the sample OHP1/*c*-Si, which is consistent with the conclusions obtained during AFM studies.

Cole-Cole plots of the sample OHP1/*c*-Si, measured in the dark and under illumination, are presented in Figure 4, *a, b* and *c*. Similar graphs for the sample OHP2/*c*-Si under different conditions can be shown in Figure 5, *a* and *b*. The Cole−Cole graph for pure sample *c*-Si in the dark is shown in Figure 6. These graphs reflect impedance characteristic data, where Im (Ω) denotes the imaginary part of the reactance, and Re (Ω) — the real part of the resistance. The semicircle in the graphs at high frequencies is associated with charge transfer and recombination through the structure/contacts, while the semicircle in the graphs at low frequencies is associated with charge carrier recombination, dielectric relaxation, and ion migration in the layers of the structure. The impedance characteristic of the sample OHP1/*c*-Si in the dark is characterized by the presence of two half-arcs, which may indicate two different mechanisms determining the transfer processes in the sample. Each half-arc may represent a different mechanism, such as charge exchange or ion diffusion, occurring on different time scales or at different energy levels. When illuminated, the number of half-arcs is reduced to one, which indicates a change in the dominant transport mechanisms in the material. This may be due to changes in the concentration of charge carriers and the recombination rate upon illumination of the sample.

One may expect that the conductivity of the OHP1/*c*-Si sample will increase upon illumination due to the photogeneration of additional charge carriers (electrons and holes). However, in this case, the opposite situation was observed: the conductivity of the OHP1/*c*-Si sample under illumination turned out to be lower than in the dark. This may be due to photoinduced defects (defects in the perovskite structure formed under the influence of light that act as trapping sites for charge carriers,

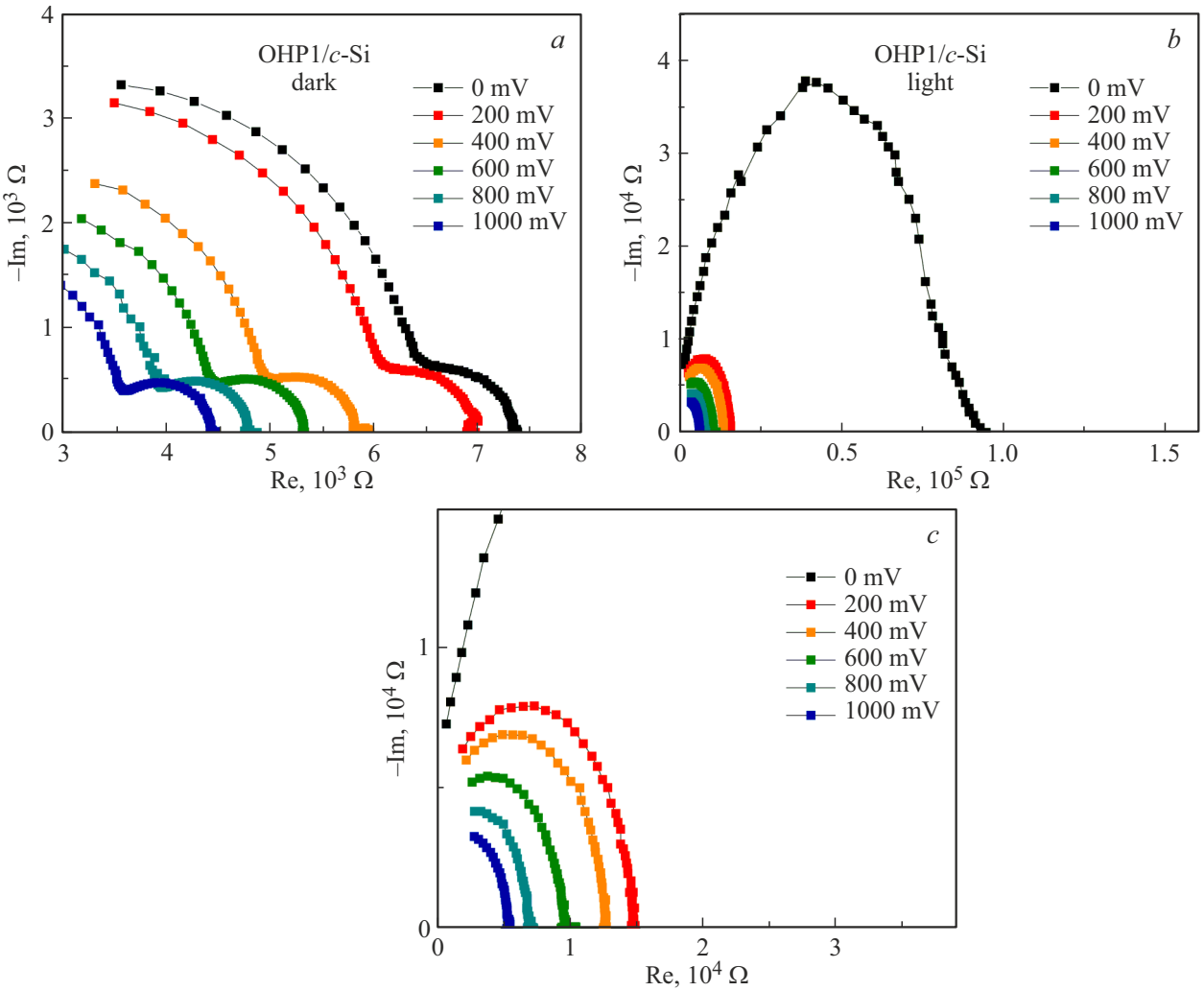

Figure 4. Impedance characteristics of the sample OHP1/*c*-Si when applying different voltages in the dark (*a*) and in the light (*b*, *c*) in environmental conditions.

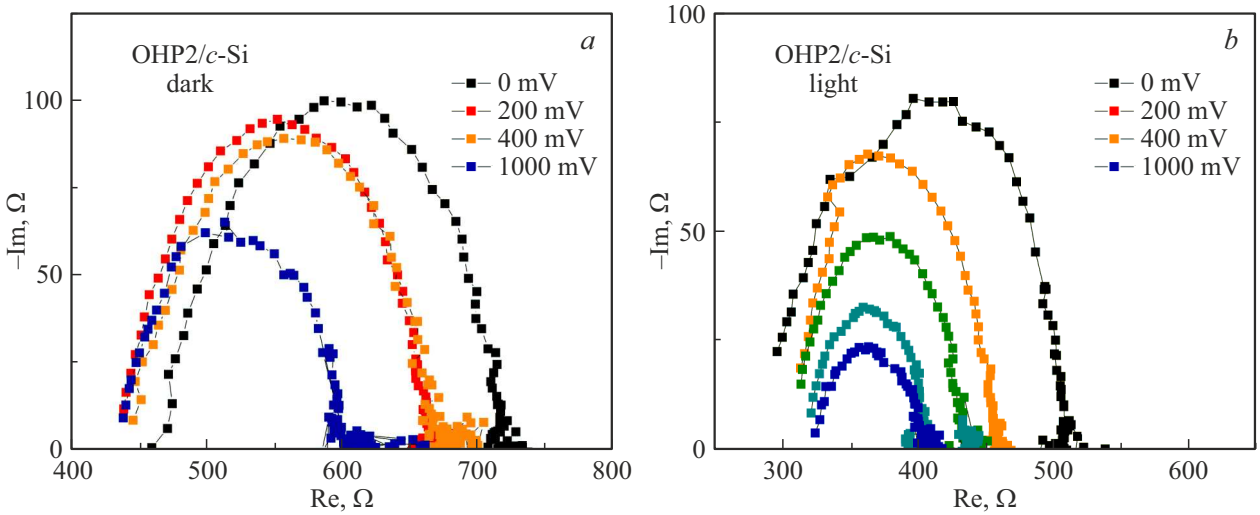

Figure 5. Impedance characteristics of the sample OHP2/*c*-Si when applying different voltages in the dark (*a*) and in the light (*b*) under environmental conditions.

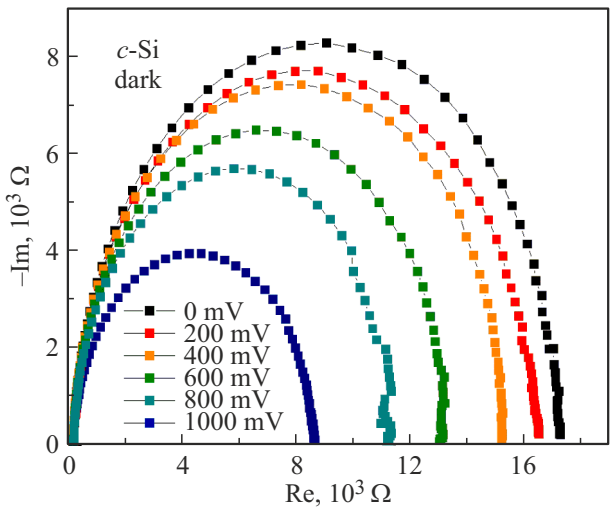

Figure 6. Impedance of characteristic of sample *c*-Si when applying different voltages in the dark under environmental conditions.

increasing recombination and decreasing conductivity) and ion migration (this process can change the local electric field and affect conductivity).

Compared with the *c*-Si sample, the OHP1/*c*-Si sample exhibits better conductivity in the dark, which is consistent with I-Vs results. Unlike *c*-Si sample, the half-arc on the impedance plot for the OHP2/*c*-Si sample does not start from 0 Ω. This may indicate the presence of additional resistance or barrier at the interface between the organometallic perovskite and silicon. The reason for this additional resistance may be surface conditions at the interface between the perovskite and silicon, oxidation processes, or the formation of insulating layer at this interface. It is also possible that there are inhomogeneities and defects in the perovskite structure. Heterogeneous interfaces between perovskite and silicon can cause different charge transfer mechanisms, which in turn can lead to a broken half-arc shape in the impedance diagram of the OHP2/*c*-Si sample. At the same time, a smooth half-

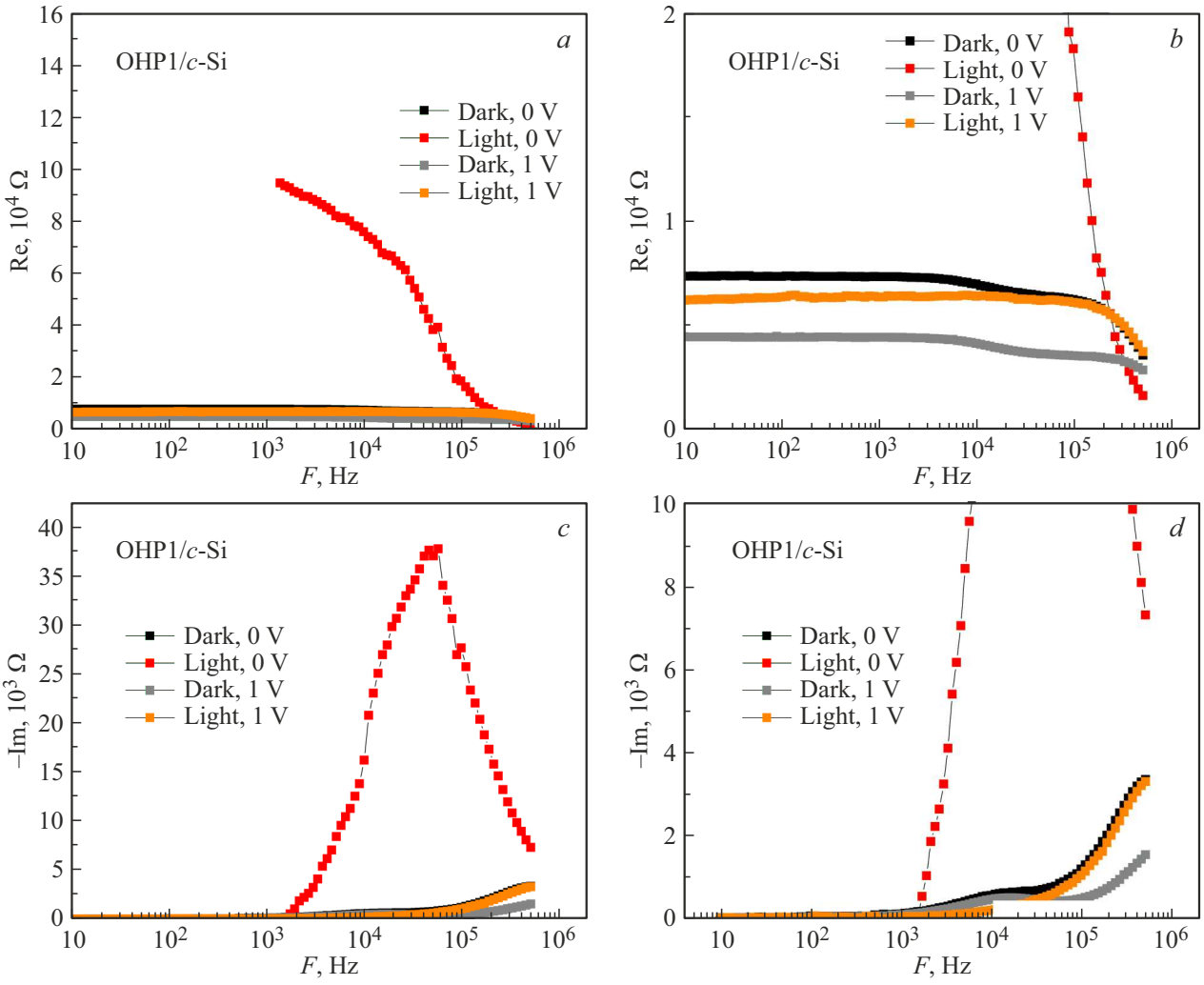

Figure 7. Frequency dependences of the real (*a*, *b*) and imaginary (*c*, *d*) parts of the impedance characteristic of the sample OHP1/*c*-Si when voltage is applied in the dark and when illuminated under environmental conditions.

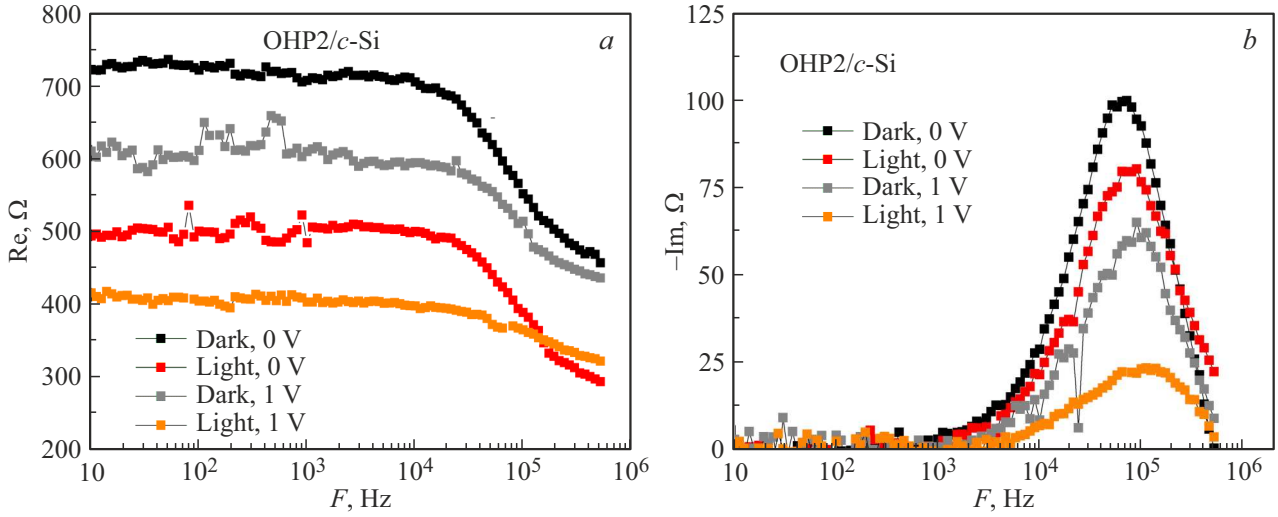

Figure 8. Frequency dependences of the real (*a*) and imaginary (*b*) parts of the impedance characteristics of the sample OHP2/*c*-Si when voltage is applied in the dark and when illuminated under environmental conditions.

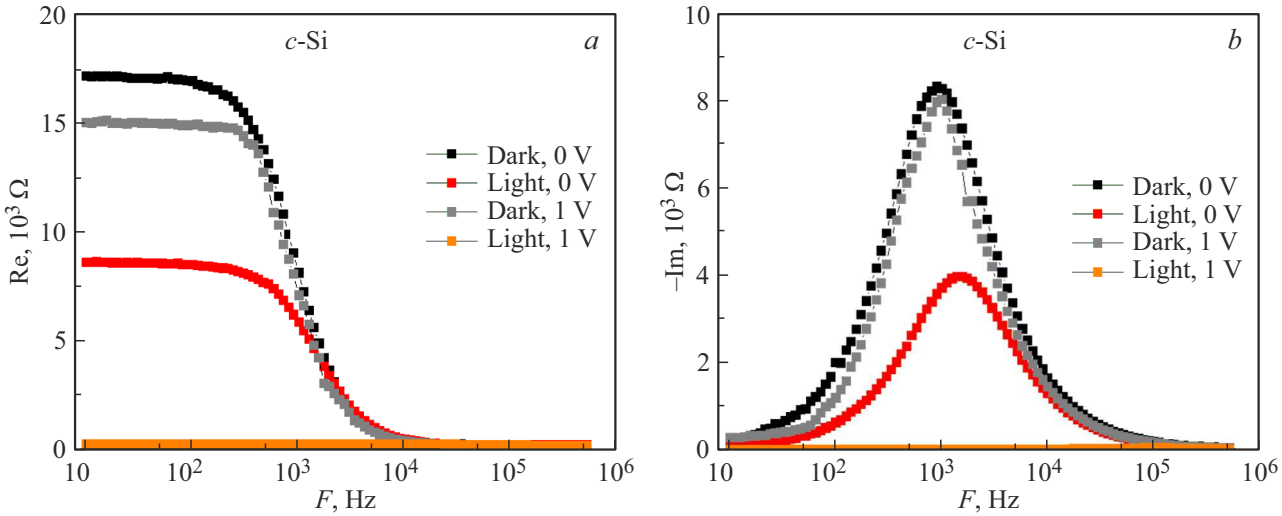

Figure 9. Frequency dependences of the real (*a*) and imaginary (*b*) parts of the impedance characteristics of the sample *c*-Si when voltage is applied in the dark and when illuminated under environmental conditions.

arc on the impedance graph of the *c*-Si sample may indicate a stable and uniform charge transfer process in such a material. It is worth noting that the conductivity of OHP2/*c*-Si sample significantly exceeds the conductivity of *c*-Si sample, which is consistent with I-Vs results. As expected, the conductivity of OHP2/*c*-Si sample increases when it is illuminated.

Frequency dependences of the real (*a*) and imaginary (*b*) parts of the impedance characteristic of structure OHP1/*c*-Si, OHP2/*c*-Si and *c*-Si when voltage is applied in the dark and when illuminated under environmental conditions are given in Figures 7, 8 and 9. As can be seen from Figures 7–9, OHP1/*c*-Si sample demonstrates better photoresponse compared to other samples, but its conductivity in light is lower than in the dark; also, its frequency dependences demonstrate a non-standard appearance. The best conductivity is demonstrated by OHP2/*c*-Si sample in comparison with other samples. For all three samples, the influence of illumination and bias voltage on the conductivity is noticeable.

The results of AFM studies of OHP1/*c*-Si and OHP2/*c*-Si samples revealed differences in the morphology of their surfaces. OHP1/*c*-Si sample has a more complex and rough morphology, which can create additional barriers to the movement of electrons and reduce the overall conductivity. At the same time, OHP2/*c*-Si sample has a smoother surface, which contributes to higher conductivity.

I-Vs of the samples showed that OHP1/*c*-Si and OHP2/*c*-Si samples have higher photoconductivity compared to *c*-Si sample, which indicates an improvement in photoconductivity due to additional layer of perovskite. The impedance characteristics of the samples also differ. The

OHP1/*c*-Si sample in the dark has two half-arcs on the impedance graph, which may indicate the presence of two different transport mechanisms in the sample, such as charge exchange or ion diffusion. When illuminated, the number of half-arcs is reduced to one, indicating change in the dominant mechanisms in the structure, possibly associated with change in the concentration of charge carriers.

4. Conclusion

In this paper, multilayer structures based on thin films of organometallic halide perovskites $CH_3NH_3PbI_3$, deposited on surfaces of SC based on crystalline silicon. The morphology and electrical properties of these structures were studied by AFM, I-Vs, and impedance spectroscopy. The studied samples demonstrated photoconductivity, and for samples with layers of perovskite OHP1/*c*-Si and OHP2/*c*-Si it significantly exceeded the values for the pure *c*-Si sample. This indicates that the organic-inorganic perovskite layer significantly improves the photoconductivity of the SC structure based on *c*-Si. It was shown that differences in the synthesis conditions of perovskites can lead to significant differences in the surface morphology and electrical properties of the samples. The results obtained make it possible to improve the performance characteristics of the next generation tandem *c*-Si SCs with top layers of organometallic halide perovskites.

Acknowledgments

The authors are grateful to E.I. Terukov and the Research Center for Thin Film Technologies in Energy for providing *c*-Si solar cells. The authors also thank I.A. Vrublevsky and A.K. Tuchkovsky for their assistance in the synthesis of organometallic perovskite materials. Regarding the synthesis of organometallic perovskites, the study was supported by a grant from the Republic of Belarus Foundation for Basic Research No. F23RNF-160 and the Russian Science Foundation No. 23-42-10029 (https://rscf.ru/project/23-42-10029/) dated 20.12.2022.

Conflict of interest

The authors declare that they have no conflict of interest.

References

[1] S. Jung, J.H. Kim, J.W. Choi, J.-W. Kang, S.H. Jin, Y. Kang, W. Song. Nanomaterials **10**, 710 (2020).
[2] Q. Chen, N. De Marco, Y. Yang, T.-B. Song, C.-C. Chen, H. Zhao, Z. Hong, H. Zhou, Y. Yang. Nano Today **10**, 355 (2015).
[3] J.H. Noh, S.H. Im, J.H. Heo, T.N. Mandal, S.I. Seo. Nano Lett. **13**, 1764 (2013).
[4] H. Oga, A. Saeki, Y. Ogomi, S. Hayase, S. Seki. J. Am. Chem. Soc. **136**, 13818 (2014).
[5] Z. Fang, Q. Zeng, C. Zuo, L. Zhang, H. Xiao, M. Cheng, L. Ding. Sci. Bull. **6**, 621 (2021).
[6] X.Y. Chin, D. Turkay, J. A. Steele, S. Tabean, S. Eswara, M. Mensi, P. Fiala, C. M. Wolff, A. Paracchino, K. Artuk, D. Jacobs, Q. Guesnay, F. Sahli, G. Andreatta, M. Boccard, Q. Jeangros, C. Ballif. Science **381**, 59 (2023).
[7] A. Guerrero, J. Bisquert, G. Garcia-Belmont. Chem. Rev. **121**, 14430 (2021).
[8] E. Hauff, D. Klotz. J. Mater. Chem. C **10**, 742 (2022).
[9] S. Ravishankar, O. Almora, C. Echeverría-Arrondo. J. Phys. Chem. Lett. **8**, 915 (2017).
[10] G. Xing, N. Mathews, S. Sun, S.S. Lim, Y.M. Lam, M. Grätzel, T.C. Sum. Science **342**, 344 (2013).
[11] E. Terukov, A. Kosarev, A. Abramov, E. Malchukova. Solar Panels Photovoltaic Materials **5** (2018).
[12] M. Masuko, M. Shigematsu, T. Hasiguchi, D. Fujishima, M. Kai, N. Yoshimira, T. Yamaguchi, Y. Ichihashi, T. Mishima, N. Matsubara, T. Yamanishi, T. Takahama, M. Taguchi, E. Maruyama, S. Okamoto. IEEE J. Photovoltaics **4**, 1433 (2014).
[13] L. Boudjemila, A.N. Aleshin, V.M. Malyshkin, P.A. Aleshin, I.P. Shcherbakov, V.N. Petrov, E.I. Terukov. Phys. Solid State **11**, 1670 (2022).
[14] A.V. Arkhipov, G.V. Nenashev, A.N. Aleshin. Phys. Solid State **63**, 525 (2021).
[15] A.M. Ivanov, G.V. Nenashev, A.N. Aleshin. J. Mater Sci: Mater. Electron. **33**, 21666 (2022).

Translated by I.Mazurov